Coupling of Cdc20 inhibition and activation by BubR1

Jamin B. Hein[1], Dimitriya H. Garvanska[1], Isha Nasa[2], Arminja Kettenbach[2], Jakob Nilsson[1,3]

[1] Novo Nordisk Foundation Center for Protein Research, Faculty of Health and Medical Science, Blegdamsvej 3B, 2200 Copenhagen

[2] Biochemistry and Cell Biology, Geisel School of Medicine at Dartmouth College

[3] Correspondence to: jakob.nilsson@cpr.ku.dk

Running title: Cdc20 dephosphorylation by PP2A complexes

Abstract

Tight regulation of the APC/C-Cdc20 ubiquitin ligase that targets Cyclin B1 for degradation is important for mitotic fidelity. The spindle assembly checkpoint (SAC) inhibits Cdc20 through the mitotic checkpoint complex (MCC). In addition, phosphorylation of Cdc20 by Cyclin B1-Cdk1 independently inhibits APC/C-Cdc20 activation. This creates a conundrum for how Cdc20 gets activated prior to Cyclin B1 degradation. Here we show that the MCC component BubR1 harbours both Cdc20 inhibition and activation activities, allowing for cross-talk between the two Cdc20 inhibition pathways. Specifically BubR1 acts as a substrate specifier for PP2A-B56 to enable efficient Cdc20 dephosphorylation in the MCC. A mutant Cdc20 mimicking the dephosphorylated state escapes a mitotic checkpoint arrest arguing that restricting Cdc20 dephosphorylation to the MCC is important. Collectively our work reveals how Cdc20 can be dephosphorylated in the presence of Cyclin B1-Cdk1 activity without causing premature anaphase onset.

Introduction

Proper progression through mitosis depends on tight regulation of the Cdc20 protein, which is an activator of the Anaphase Promoting Complex/Cyclosome (APC/C), a large E3 ubiquitin ligase (Alfieri et al., 2017; Barford, 2020). The APC/C-Cdc20 complex targets several proteins for proteasomal degradation, including Cyclin B1 and Securin, which initiates anaphase by lowering Cdk1 kinase activity and release of centromere cohesion, respectively (Pines, 2011). Cdc20 activity is regulated by the spindle assembly checkpoint (SAC), which in response to unattached kinetochores delays anaphase onset by sequestering Cdc20 in the mitotic checkpoint complex (MCC)(Lara-Gonzalez et al., 2012; Musacchio, 2011; Varetti and Musacchio, 2008). The MCC is composed of Mad2-Cdc20-BubR1-Bub3, where Cdc20 is tightly bound and critical surface areas responsible for APC/C activation are blocked (Chao et al., 2012; Di Fiore et al., 2015; Di Fiore et al., 2016; Herzog et al., 2009; Sudakin et al., 2001). The kinetochore generated MCC complex binds stably to the APC/C-Cdc20 complex to generate an APC/C-MCC complex containing two Cdc20 molecules (Alfieri et al., 2016; Hein and Nilsson, 2014; Izawa and Pines, 2015; Primorac and Musacchio, 2013; Yamaguchi et al., 2016).

In addition to SAC regulation of Cdc20, we and others have shown that Cyclin B1-Cdk1 can phosphorylate a number of Thr-Pro (TP) sites in the N-terminal region of Cdc20 to block its activity (Hein et al., 2017; Hein and Nilsson, 2016; Labit et al., 2012; Yudkovsky et al., 2000). These phosphorylation sites cluster around the C-box of Cdc20, a motif that binds and activates the APC/C (Chang et al., 2014; Kimata et al., 2008). For activation of Cdc20, the TP sites must be dephosphorylated (Labit et al., 2012). We previously showed that the PP2A-B55 phosphatase is able to do so *in vitro* and in human cells (Hein et al., 2017). PP2A-B55 is a Ser/Thr phosphatase which is specifically activated at the metaphase-anaphase transition to dephosphorylate thousands of Cdk1 targets hereby driving the anaphase transition (Cundell et

al., 2016; Godfrey et al., 2017; Holder et al., 2019; Kruse et al., 2020; McCloy et al., 2015; Nilsson, 2019). PP2A-B55 activity is regulated by the Cdk1-MASTL-ARPP19 pathway in which Cdk1 activates the MASTL kinase that then phosphorylates ARPP19/ENSA proteins which bind and inactivate PP2A-B55 (Gharbi-Ayachi et al., 2010; Mochida et al., 2010; Vigneron et al., 2009). The activation of PP2A-B55 is initiated by a decrease of Cdk1 activity which activates PP1 to initiate dephosphorylation and inactivation of the MASTL kinase (Heim et al., 2015; Ma et al., 2016; Rogers et al., 2016).

This generates a conundrum because Cdc20 needs to be dephosphorylated before PP2A-B55 can become active. One solution to this problem could be that another protein phosphatase activates Cdc20 prior to PP2A-B55, but this would potentially lead to premature activation of Cdc20 and deregulation of cell division. Here we provide a solution by showing that both PP2A-B55 and PP2A-B56 are phosphatases for Cdc20. PP2A-B56 is active in prometaphase and through binding to BubR1, it selectively dephosphorylates Cdc20 within the MCC thereby priming the inhibited pool of Cdc20 for APC/C activation prior to PP2A-B55 activation.

Results and discussion

A screen for PP2A-B56 mitotic substrates identifies Cdc20

We recently developed a method to identify substrates of specific protein phosphatases during mitosis (Fig. 1A)(Kruse et al., 2020). Briefly, nocodazole arrested cells are harvested and lysed in the presence of a specific inhibitor of a protein phosphatase. As ATP is rapidly depleted this inactivates kinases while protein phosphatases are still active unless an inhibitor is present. The lysis reaction is then incubated at 30 degrees for 5 minutes and the reaction is stopped. Proteins are precipitated, digested with trypsin followed by phosphopeptide enrichment and analysis by LC-MS/MS. For specific inhibition of PP2A-B56, we employed a high affinity LxxIxE motif containing peptide that prevents the phosphatase from binding to all its substrates (Hertz et al., 2016; Kruse et al., 2018; Kruse et al., 2020). As a control, we used an AxxAxE peptide that does not bind the phosphatase. This screen identified 54 phosphorylation sites that significantly increased (log2 ratio LxxIxE/AxxAxE > 0.7, p-value <0.05) in lysates treated with LxxIxE peptide versus AxxAxE peptide (Fig 1B-C, Supplemental Table 1). Several of the regulated sites were in proteins already known to be PP2A-B56 substrates that contain validated LxxIxE motifs (Fig. 1D). As an example, Kif4A T799 and ADAM17 T735 are known targets of PP2A-B56 and these two proteins contain validated LxxIxE motifs (Bastos et al., 2014; Kruse et al., 2020; Wang et al., 2020). Furthermore, RacGAP1 S203, BubR1 T508 and ESPL1 S1475 are close to validated LxxIxE motifs supporting the strength of the screening approach. In addition, we identified PP2A-B56 regulated phosphorylation sites in proteins containing bioinformatically predicted LxxIxE motifs as well as proteins with no motifs (Fig. 1E). One phosphorylation site that caught our attention was Cdc20 T70, which is a Cdk1 phosphorylation site known to block Cdc20 activation of the APC/C. We have previously found this phosphorylation site to be a substrate of PP2A-B55 so we decided to investigate the role of PP2A-B56 in regulating this site in more detail.

Two distinct mitotic PP2A complexes can dephosphorylate Cdc20

We first confirmed that PP2A-B56 can regulate Cdc20 T70 phosphorylation in cells. We depleted all B56 regulatory subunits,arrested cells in nocodazole, immunopurified Cdc20 and analysed T70 phosphorylation levels by quantitative western blotting (LiCor) (Fig. 2A). Indeed, we observed increased levels of Cdc20 T70 in nocodazole arrested cells when B56 subunits were depleted. The level of co-purifying APC3 and its phosphorylation on T447, a Cdk1 site, was not affected by B56 depletion. We then treated cells with the Cdk1 inhibitor RO3306 to determine if PP2A-B56 was required for Cdc20 T70 dephosphorylation when cells exit mitosis. However, we observed efficient dephosphorylation in the absence of PP2A-B56 arguing that other protein phosphatases can dephosphorylate Cdc20 T70 (Fig. 2A).

To investigate this, we turned to the lysate system, where we can add specific phosphatase inhibitors for a short time avoiding indirect effects from long-term perturbation by siRNA depletion. We analysed Cdc20 T70 phosphorylation and compared this to APC3 T447 phosphorylation in the presence of specific phosphatase inhibitors. We used thiophosphorylated Arpp19 to inhibit PP2A-B55, Nipp1 to inhibit PP1 (Winkler et al., 2015) and the LxxIxE peptide to inhibit PP2A-B56. This experiment revealed that both Arpp19 and LxxIxE but not the corresponding controls delayed Cdc20 T70 dephosphorylation (Fig. 2B). In contrast, APC3 T447 dephosphorylation was only inhibited by Arpp19 (Fig. 2C). Strikingly addition of both Arpp19 and LxxIxE peptide was required to strongly block Cdc20 T70 dephosphorylation. This shows that both PP2A-B55 and PP2A-B56 are able to dephosphorylate Cdc20 T70, explaining how Cdc20 gets dephosphorylated in cells depleted of PP2A-B56 upon addition of a Cdk1 inhibitor.

The results show that two distinct PP2A complexes can dephosphorylate Cdc20 with PP2A-B56 likely acting during prometaphase and PP2A-B55 during anaphase.

BubR1 acts as a substrate specifier for PP2A-B56 to dephosphorylate Cdc20

Our data argue that Cdc20 T70 dephosphorylation is dependent on PP2A-B56 binding to an LxxIxE motif. This is consistent with the *in vitro* dephosphorylation data we recently published where we showed that Cdc20 inhibitory Cdk1 phosphorylation's can be dephosphorylated by PP2A-B56 when an LxxIxE motif is fused to Cdc20 (Kruse et al., 2020). Although PP2A-B56 works inefficiently on Cdk1 sites, the presence of LxxIxE motifs can overcome this inefficiency by positioning the phosphatase in the proximity of the Cdk1 sites.

To establish the relevant LxxIxE motif for PP2A-B56 mediated Cdc20 dephosphorylation in cells, we focused on proteins known to bind Cdc20. BubR1 contains a functional LxxIxE motif (L669-E674) and through its N-terminus, BubR1 binds tightly to the C-terminal WD40 domain of Cdc20. We therefore investigated if PP2A-B56 bound to BubR1 could be responsible for Cdc20 T70 dephosphorylation. We used stable HeLa cell lines expressing siRNA resistant Venus tagged BubR1 WT and L669A/I672A (BubR1 2A) and immunopurified Cdc20 from these (Kruse et al., 2013). The parental cell line or the cell lines expressing exogenous BubR1were treated with BubR1 RNAi and arrested in mitosis using nocodazole (note that there is some slippage from the mitotic arrest in the samples expressing exogenous BubR1). The level of Cdc20 T70 and APC3 T447 phosphorylation was then determined by quantitative immunoblotting (Fig. 3A). In the purifications from Venus BubR1 2A expressing cells, we observed a specific increase in Cdc20 T70 levels while APC3 T447 levels were similar to BubR1 WT. This experiment shows that binding of PP2A-B56 to BubR1 is important for Cdc20 dephosphorylation.

The results raised the possibility that Cdc20 as part of the MCC would be specifically dephosphorylated by PP2A-B56. To test this model, we immunopurified different Cdc20 pools from nocodazole arrested cells (Fig. 3B). We purified total Cdc20 using two different

antibodies (reflecting free Cdc20 + MCC bound Cdc20) as well as Cdc20 associated with BubR1 and APC/C (reflecting MCC and APC/C-MCC complexes). Compared to total Cdc20, we observed less Cdc20 T70 phosphorylation in BubR1 and APC4 purifications in line with our results on Venus BubR1 2A. The degree of APC3 T447 phosphorylation was similar in all samples arguing for a specific effect on Cdc20.

Collectively these results show that BubR1 bound PP2A-B56 can dephosphorylate Cdc20 T70. This selective dephosphorylation leads to lower Cdc20 T70 phosphorylation in MCC and APC/C-MCC complexes.

Cdk1 phosphorylation of Cdc20 is required for a prolonged mitotic arrest.

Our results support a model in which Cdc20 is selectively dephosphorylated as part of MCC complexes. This raised the question of whether dephosphorylation of Cdc20 not inhibited by the MCC would result in premature activation of APC/C-Cdc20. To investigate this, we analysed the effect of expressing a variant of Cdc20 (Cdc20 3AA – T70, T59 and T55 mutated to AA) that cannot be phosphorylated by Cdk1 on a nocodazole induced mitotic arrest (Hein et al., 2017). Cells stably expressing YFP-tagged or untagged Cdc20 variants and depleted of endogenous Cdc20 were followed by time-lapse microscopy and escape from the arrest recorded (Fig. 4A-B, Supplemental Fig.1). Strikingly a large fraction of Cdc20 AA expressing cells escaped the mitotic arrest while Cdc20 WT and Cdc20 3DD stayed arrested. We further analysed the effect of Cdk1 phosphorylation of Cdc20 using mutants of Cdc20 that cannot form the MCC (Cdc20 R132A and 4A)(Lischetti et al., 2014). With both these Cdc20 mutants, we observed a faster exit when Cdk1 phosphorylation was prevented (Fig. 4C-D). This argues that Cdk1 phosphorylation of Cdc20 contributes to maintaining a mitotic arrest independently of the SAC.

In summary, our work explains how Cdc20 can be dephosphorylated even in the presence of high levels of Cyclin B1-Cdk1. By coupling Cdc20 dephosphorylation to an MCC component, this ensures that dephosphorylated Cdc20 is kept inactive but ready to activate the APC/C once the SAC is satisfied. Our data also suggests that Cdc20 phosphorylation prevents unscheduled activation during a mitotic arrest possibly by inactivating Cdc20 not bound to MCC components. Recent work from the Yamano lab using *X. laevis* embryonic extracts identified PP2A-B56 as a Cdc20 phosphatase consistent with our work (Fujimitsu and Yamano, 2020). Their work showed that an LxxIxE motif in APC1 binds to PP2A-B56 to mediate efficient Cdc20 binding, although the level of Cdc20 phosphorylation was not analysed. We have not explored this motif, but since the *X. laevis* extract lacks a functional SAC, BubR1 cannot act as a substrate specifier for PP2A-B56 in this system. We note that APC1 mutants that cannot bind PP2A-B56 progress with almost wild type kinetics into anaphase which suggests that another phosphatase can activate Cdc20. Based on our results, we favour that this is PP2A-B55. A recent study also implicated PP1 in Cdc20 T70 dephosphorylation in human cells in line with work from *C. elegans* showing PP1 as a Cdc20 phosphatase (Bancroft et al., 2020; Kim et al., 2017). The results from human somatic cells could be an indirect effect of PP1 inhibition leading to delayed PP2A-B55 activation. In our lysate experiment, we see no effect on Cdc20 T70 phosphorylation upon PP1 inhibition by Nipp1. In agreement with this, depletion of PP1alpha/gamma showed limited effect on Cdc20 T70 dephosphorylation in cells (Bancroft et al., 2020). However, further work is needed to clarify if PP1 can dephosphorylate Cdc20 in cells.

We favour that in the absence of PP2A-B56 mitotic exit through Cdc20 dephosphorylation is possible and can be driven by PP2A-B55. This redundancy in Cdc20 phosphatases can explain the limited effect on a forced mitotic exit in cells expressing BubR1 unable to bind PP2A-B56 (Espert et al., 2014; Nijenhuis et al., 2014). However, in unperturbed conditions Cdc20

dephosphorylation by BubR1-PP2A-B56 is likely required for efficient onset of anaphase allowing a drop in Cyclin B1 levels and thus PP2A-B55 activation. This activation of PP2A-B55 would then further activate APC/C-Cdc20 to ensure a rapid metaphase-anaphase transition.

Collectively our work provides important insight into the regulation of Cdc20 and reveals that BubR1 integrates both inhibitory and activating activities.

Acknowledgements

Work at the Novo Nordisk Foundation Center for Protein Research is supported by grant NNF14CC0001 and JN is supported by grants from the Danish Cancer Society (R167-A10951-17-S2), Independent Research Fund Denmark (DFF-4183-00388 and 8021-00101B) and Novo Nordisk Foundation (NNF16OC0022394 and NNF18OC0053124). JBH was funded by grant NNF17OC0025404 from the Novo Nordisk Foundation and the Stanford Bio-X Program. A.N.K was supported by grants from NIH/NIGMS (R35GM119455). The Orbitrap Fusion Tribrid mass spectrometer was acquired with support from NIH (S10-OD016212).

Conflict of interest

The authors have no conflict of interest

Figure legends

Figure 1. A screen for mitotic PP2A-B56 substrates identifies Cdc20

A) A schematic of the approach used to identify PP2A-B56 substrates in nocodazole arrested cells. **B**) Summary of the screen results categorising sites based on the presence of validated or predicted LxxIxE motifs **C**) Log2 ratio of regulated phosphorylation sites versus p-value. Sites in proteins with validated LxxIxE motifs indicated with protein names as well as Cdc20 T70. **D-E**) Examples of identified sites in the screen and whether they contain validated, predicted or no LxxIxE motifs.

Figure 2. PP2A-B56 and PP2A-B55 are phosphatases for Cdc20 T70

A) Cells treated with a control RNAi oligo or a pool of B56 RNAi oligoes targeting all isoforms were arrested in nocodazole and Cdc20 immunopurified. Samples were analysed by western blot for Cdc20 T70p and APC3 T447p as well as APC3 and BubR1. The degree of Cdc20 T70p and APC3 T447p was determined by normalising to pan Cdc20 or pan APC3 signals. **B-C**) A nocodazole lysate was prepared and treated with the indicated phosphatase inhibitors (see also Fig.1A) for 5 minutes or 15 minutes as indicated. Cdc20 or APC4 was immunopurified and the level of Cdc20 T70p and APC3 T447p determined. For all experiments 3 independent experiments where conducted and quantified.

Figure 3. Cdc20 T70 is dephosphorylated by BubR1 bound PP2A-B56

A) Schematic indicating Cdc20 and PP2A-B56 binding to BubR1. The mutations in BubR1 2A is indicated. B) Stable cell lines expressing Venus-BubR1 WT or 2A were depleted of BubR1 by RNAi and arrested in mitosis with nocodazole. Cdc20 was immunopurified from the cells and the degree of Cdc20 T70p and APC3 T447p determined. The samples were compared to similar samples from the parental cells not treated with BubR1 RNAi. **B**) Cdc20, BubR1 and

APC4 were immunopurified from nocodazole arrested cells and the level of Cdc20 T70p and APC3 T447p determined. For Cdc20 two different antibodies were used. For all experiments at least 3 independent experiments where conducted and quantified.

Figure 4. Cdk1 phoshorylation of Cdc20 is required for an efficient mitotic arrest in response to microtubule poisons

A) Live cell imaging of Hela cells depleted of endogenous Cdc20 and transiently expressing untagged Cdc20 WT, 3DD or 3AA in the presence of nocadazole (30 ng/ml). Percent of cells that exit mitosis during the course of imaging from three independent experiments (mean and SD indicated). **B**) As in A) Time from NEBD to mitotic exit or end of filming from three independent experiments (each dot represents a single cell, red line indicates mean and SD, n values are shown in the graph and represent single cells analysed per condition). **C**) Live cell imaging of stable cell lines that were depleted of endogenous Cdc20 and expressing indicated YFP tagged Cdc20 proteins in the presence of nocodazole (30 ng/ml). The R132A mutation prevents Mad2 binding while the 4A mutations prevent BubR1 binding. Time from NEBD to mitotic exit (each dot represents a single cell, red line indicates mean and standard deviation, n values are shown in the graph and represent single cells analysed per condition). D) Model: MCC bound BubR1 is preferentially dephosphorylated by PP2A-B56, whereas free Cdc20 is phosphorylated by Cdk1.

Supplementary Figure 1.

A) Representative images of live cell imaging of Hela cells depleted of endogenous Cdc20 and complemented with indicated forms of YFP tagged Cdc20. **B**) Quantification of cells that exit mitosis in the presence of nocodazole (30 ng/ml) during live cell imaging as in A). Percent of cells from three independent experiments (mean and SD indicated). **C**) Hela cells depleted of

endogenous Cdc20 and complemented with indicated forms of YFP-tagged Cdc20 in the presence of nocodazole (30 ng/ml, when indicated). Time from NEBD to mitotic exit or end of filming from three independent experiments (each dot represents a single cell, red line indicates mean and standard deviation).

References

Alfieri, C., L. Chang, Z. Zhang, J. Yang, S. Maslen, M. Skehel, and D. Barford. 2016. Molecular basis of APC/C regulation by the spindle assembly checkpoint. *Nature*. 536:431-436.

Alfieri, C., S. Zhang, and D. Barford. 2017. Visualizing the complex functions and mechanisms of the anaphase promoting complex/cyclosome (APC/C). *Open Biol*. 7.

Bancroft, J., J. Holder, Z. Geraghty, T. Alfonso-Perez, D. Murphy, F.A. Barr, and U. Gruneberg. 2020. PP1 promotes cyclin B destruction and the metaphase-anaphase transition by dephosphorylating CDC20. *Mol Biol Cell*. 31:2315-2330.

Barford, D. 2020. Structural interconversions of the anaphase-promoting complex/cyclosome (APC/C) regulate cell cycle transitions. *Curr Opin Struct Biol*. 61:86-97.

Bastos, R.N., M.J. Cundell, and F.A. Barr. 2014. KIF4A and PP2A-B56 form a spatially restricted feedback loop opposing Aurora B at the anaphase central spindle. *J Cell Biol*. 207:683-693.

Chang, L.F., Z. Zhang, J. Yang, S.H. McLaughlin, and D. Barford. 2014. Molecular architecture and mechanism of the anaphase-promoting complex. *Nature*. 513:388-393.

Chao, W.C., K. Kulkarni, Z. Zhang, E.H. Kong, and D. Barford. 2012. Structure of the mitotic checkpoint complex. *Nature*. 484:208-213.

Cundell, M.J., L.H. Hutter, R. Nunes Bastos, E. Poser, J. Holder, S. Mohammed, B. Novak, and F.A. Barr. 2016. A PP2A-B55 recognition signal controls substrate dephosphorylation kinetics during mitotic exit. *J Cell Biol*. 214:539-554.

Di Fiore, B., N.E. Davey, A. Hagting, D. Izawa, J. Mansfeld, T.J. Gibson, and J. Pines. 2015. The ABBA motif binds APC/C activators and is shared by APC/C substrates and regulators. *Dev Cell*. 32:358-372.

Di Fiore, B., C. Wurzenberger, N.E. Davey, and J. Pines. 2016. The Mitotic Checkpoint Complex Requires an Evolutionary Conserved Cassette to Bind and Inhibit Active APC/C. *Mol Cell*. 64:1144-1153.

Espert, A., P. Uluocak, R.N. Bastos, D. Mangat, P. Graab, and U. Gruneberg. 2014. PP2A-B56 opposes Mps1 phosphorylation of Knl1 and thereby promotes spindle assembly checkpoint silencing. *J Cell Biol*. 206:833-842.

Foley, E.A., M. Maldonado, and T.M. Kapoor. 2011. Formation of stable attachments between kinetochores and microtubules depends on the B56-PP2A phosphatase. *Nat Cell Biol*. 13:1265-1271.

Fujimitsu, K., and H. Yamano. 2020. PP2A-B56 binds to Apc1 and promotes Cdc20 association with the APC/C ubiquitin ligase in mitosis. *EMBO Rep*. 21:e48503.

Gharbi-Ayachi, A., J.C. Labbe, A. Burgess, S. Vigneron, J.M. Strub, E. Brioudes, A. Van-Dorsselaer, A. Castro, and T. Lorca. 2010. The substrate of Greatwall kinase, Arpp19, controls mitosis by inhibiting protein phosphatase 2A. *Science*. 330:1673-1677.

Godfrey, M., S.A. Touati, M. Kataria, A. Jones, A.P. Snijders, and F. Uhlmann. 2017. PP2A(Cdc55) Phosphatase Imposes Ordered Cell-Cycle Phosphorylation by Opposing Threonine Phosphorylation. *Mol Cell*. 65:393-402 e393.

Grassetti, A.V., R. Hards, and S.A. Gerber. 2017. Offline pentafluorophenyl (PFP)-RP prefractionation as an alternative to high-pH RP for comprehensive LC-MS/MS proteomics and phosphoproteomics. *Anal Bioanal Chem*. 409:4615-4625.

Heim, A., A. Konietzny, and T.U. Mayer. 2015. Protein phosphatase 1 is essential for Greatwall inactivation at mitotic exit. *EMBO Rep*. 16:1501-1510.

Hein, J.B., E.P.T. Hertz, D.H. Garvanska, T. Kruse, and J. Nilsson. 2017. Distinct kinetics of serine and threonine dephosphorylation are essential for mitosis. *Nat Cell Biol*. 19:1433-1440.

Hein, J.B., and J. Nilsson. 2014. Stable MCC binding to the APC/C is required for a functional spindle assembly checkpoint. *EMBO Rep*. 15:264-272.

Hein, J.B., and J. Nilsson. 2016. Interphase APC/C-Cdc20 inhibition by cyclin A2-Cdk2 ensures efficient mitotic entry. *Nat Commun*. 7:10975.

Hertz, E.P.T., T. Kruse, N.E. Davey, B. Lopez-Mendez, J.O. Sigurethsson, G. Montoya, J.V. Olsen, and J. Nilsson. 2016. A Conserved Motif Provides Binding Specificity to the PP2A-B56 Phosphatase. *Mol Cell*. 63:686-695.

Herzog, F., I. Primorac, P. Dube, P. Lenart, B. Sander, K. Mechtler, H. Stark, and J.M. Peters. 2009. Structure of the anaphase-promoting complex/cyclosome interacting with a mitotic checkpoint complex. *Science*. 323:1477-1481.

Holder, J., E. Poser, and F.A. Barr. 2019. Getting out of mitosis: spatial and temporal control of mitotic exit and cytokinesis by PP1 and PP2A. *FEBS Lett*. 593:2908-2924.

Izawa, D., and J. Pines. 2015. The mitotic checkpoint complex binds a second CDC20 to inhibit active APC/C. *Nature*. 517:631-634.

Kim, T., P. Lara-Gonzalez, B. Prevo, F. Meitinger, D.K. Cheerambathur, K. Oegema, and A. Desai. 2017. Kinetochores accelerate or delay APC/C activation by directing Cdc20 to opposing fates. *Genes Dev*. 31:1089-1094.

Kimata, Y., J.E. Baxter, A.M. Fry, and H. Yamano. 2008. A role for the Fizzy/Cdc20 family of proteins in activation of the APC/C distinct from substrate recruitment. *Mol Cell*. 32:576-583.

Kruse, T., N. Biedenkopf, E.P.T. Hertz, E. Dietzel, G. Stalmann, B. Lopez-Mendez, N.E. Davey, J. Nilsson, and S. Becker. 2018. The Ebola Virus Nucleoprotein Recruits the Host PP2A-B56 Phosphatase to Activate Transcriptional Support Activity of VP30. *Mol Cell*. 69:136-145 e136.

Kruse, T., S.P. Gnosa, I. Nasa, D.H. Garvanska, J.B. Hein, H. Nguyen, J. Samsoe-Petersen, B. Lopez-Mendez, E.P.T. Hertz, J. Schwarz, H.S. Pena, D. Nikodemus, M. Kveiborg, A.N. Kettenbach, and J. Nilsson. 2020. Mechanisms of site-specific dephosphorylation and kinase opposition imposed by PP2A regulatory subunits. *EMBO J*. 39:e103695.

Kruse, T., G. Zhang, M.S. Larsen, T. Lischetti, W. Streicher, T. Kragh Nielsen, S.P. Bjorn, and J. Nilsson. 2013. Direct binding between BubR1 and B56-PP2A phosphatase complexes regulate mitotic progression. *J Cell Sci*. 126:1086-1092.

Labit, H., K. Fujimitsu, N.S. Bayin, T. Takaki, J. Gannon, and H. Yamano. 2012. Dephosphorylation of Cdc20 is required for its C-box-dependent activation of the APC/C. *EMBO J*. 31:3351-3362.

Lara-Gonzalez, P., F.G. Westhorpe, and S.S. Taylor. 2012. The spindle assembly checkpoint. *Curr Biol*. 22:R966-980.

Lischetti, T., G. Zhang, G.G. Sedgwick, V.M. Bolanos-Garcia, and J. Nilsson. 2014. The internal Cdc20 binding site in BubR1 facilitates both spindle assembly checkpoint signalling and silencing. *Nat Commun*. 5:5563.

Ma, S., S. Vigneron, P. Robert, J.M. Strub, S. Cianferani, A. Castro, and T. Lorca. 2016. Greatwall dephosphorylation and inactivation upon mitotic exit is triggered by PP1. *J Cell Sci*. 129:1329-1339.

McAlister, G.C., D.P. Nusinow, M.P. Jedrychowski, M. Wuhr, E.L. Huttlin, B.K. Erickson, R. Rad, W. Haas, and S.P. Gygi. 2014. MultiNotch MS3 enables accurate, sensitive, and multiplexed detection of differential expression across cancer cell line proteomes. *Anal Chem*. 86:7150-7158.

McCloy, R.A., B.L. Parker, S. Rogers, R. Chaudhuri, V. Gayevskiy, N.J. Hoffman, N. Ali, D.N. Watkins, R.J. Daly, D.E. James, T. Lorca, A. Castro, and A. Burgess. 2015. Global Phosphoproteomic Mapping of Early Mitotic Exit in Human Cells Identifies Novel Substrate Dephosphorylation Motifs. *Mol Cell Proteomics*. 14:2194-2212.

Mochida, S., S.L. Maslen, M. Skehel, and T. Hunt. 2010. Greatwall phosphorylates an inhibitor of protein phosphatase 2A that is essential for mitosis. *Science*. 330:1670-1673.

Musacchio, A. 2011. Spindle assembly checkpoint: the third decade. *Philos Trans R Soc Lond B Biol Sci*. 366:3595-3604.

Nijenhuis, W., G. Vallardi, A. Teixeira, G.J. Kops, and A.T. Saurin. 2014. Negative feedback at kinetochores underlies a responsive spindle checkpoint signal. *Nat Cell Biol*. 16:1257-1264.

Nilsson, J. 2019. Protein phosphatases in the regulation of mitosis. *J Cell Biol*. 218:395-409.

Pines, J. 2011. Cubism and the cell cycle: the many faces of the APC/C. *Nat Rev Mol Cell Biol*. 12:427-438.

Primorac, I., and A. Musacchio. 2013. Panta rhei: the APC/C at steady state. *J Cell Biol*. 201:177-189.

Rogers, S., D. Fey, R.A. McCloy, B.L. Parker, N.J. Mitchell, R.J. Payne, R.J. Daly, D.E. James, C.E. Caldon, D.N. Watkins, D.R. Croucher, and A. Burgess. 2016. PP1 initiates the dephosphorylation of MASTL, triggering mitotic exit and bistability in human cells. *J Cell Sci*. 129:1340-1354.

Senko, M.W., P.M. Remes, J.D. Canterbury, R. Mathur, Q. Song, S.M. Eliuk, C. Mullen, L. Earley, M. Hardman, J.D. Blethrow, H. Bui, A. Specht, O. Lange, E. Denisov, A. Makarov, S. Horning, and V. Zabrouskov. 2013. Novel parallelized quadrupole/linear ion trap/Orbitrap tribrid mass spectrometer improving proteome coverage and peptide identification rates. *Anal Chem*. 85:11710-11714.

Sudakin, V., G.K. Chan, and T.J. Yen. 2001. Checkpoint inhibition of the APC/C in HeLa cells is mediated by a complex of BUBR1, BUB3, CDC20, and MAD2. *J Cell Biol*. 154:925-936.

Ting, L., R. Rad, S.P. Gygi, and W. Haas. 2011. MS3 eliminates ratio distortion in isobaric multiplexed quantitative proteomics. *Nat Methods*. 8:937-940.

Varetti, G., and A. Musacchio. 2008. The spindle assembly checkpoint. *Curr Biol*. 18:R591-595.

Vigneron, S., E. Brioudes, A. Burgess, J.C. Labbe, T. Lorca, and A. Castro. 2009. Greatwall maintains mitosis through regulation of PP2A. *EMBO J*. 28:2786-2793.

Wang, X., D.H. Garvanska, I. Nasa, Y. Ueki, G. Zhang, A.N. Kettenbach, W. Peti, J. Nilsson, and R. Page. 2020. A dynamic charge-charge interaction modulates PP2A:B56 substrate recruitment. *Elife*. 9.

Winkler, C., S. De Munter, N. Van Dessel, B. Lesage, E. Heroes, S. Boens, M. Beullens, A. Van Eynde, and M. Bollen. 2015. The selective inhibition of protein phosphatase-1 results in mitotic catastrophe and impaired tumor growth. *J Cell Sci*. 128:4526-4537.

Yamaguchi, M., R. VanderLinden, F. Weissmann, R. Qiao, P. Dube, N.G. Brown, D. Haselbach, W. Zhang, S.S. Sidhu, J.M. Peters, H. Stark, and B.A. Schulman. 2016. Cryo-EM of Mitotic Checkpoint Complex-Bound APC/C Reveals Reciprocal and Conformational Regulation of Ubiquitin Ligation. *Mol Cell*. 63:593-607.

Yudkovsky, Y., M. Shteinberg, T. Listovsky, M. Brandeis, and A. Hershko. 2000. Phosphorylation of Cdc20/fizzy negatively regulates the mammalian cyclosome/APC in the mitotic checkpoint. *Biochem Biophys Res Commun*. 271:299-304.

Materials and methods

Cloning

As described previously in Hein et al 2017 (Hein et al., 2017) . In short, full length Cdc20 was amplified by PCR and cloned into the BamHI and NotI sites of pcDNA5/FRT/TO 3*FLAG-Venus. Synthetic DNA corresponding to the first 344 nucleotides of Cdc20 with T55, T59 and T70 changed to either alanine (3AA) or aspartic acid (3DD) was ordered from GeneArt and assembled by two step PCR and cloned into BamHI and NotI sites of pcDNA5/FRT/TO 3*FLAG-Venus. The Cdc20 sequence was made resistant to the Cdc20 RNAi oligo by introducing silent mutations by quick change PCR. RNAi resistant Cdc20 WT, 3AA and 3DD was cloned into Xho1 and BamH1 site of pIRES-AcGFP1 (Clonetech).

BubR1 WT and 2A are described in Kruset et al 2013 (Kruse et al., 2013). Cdc20 R132A and 4A described in Lischetti et al 2014(Lischetti et al., 2014).

Antibodies.

The following antibodies were used at the indicated dilutions for western blot. Cdc20 mouse monoclonal (sc-13162, 1:1000, Santa Cruz, clone E7, indicated as #1), Cdc20 mouse monoclonal (MAB3775, Millipore, clone AR12, indicated as #2), Cdc20 T70 phosphorylation specific antibodies rabbit polyclonal (raised against peptides CSKVQT(Tp)PSKPG; Moravian Biotechnology, reference 22). APC3 T447p rabbit polyclonal (raised against Peptides CGKISTI(Tp)PQIQAF ; Moravian Biotechnology), Anti-phospho Histone H3 (Ser 10) rabbit polyclonal (06-570, 1:1000, Millipore), APC4 mouse monoclonal (Moravian, 1:500, clone CIV 1.1), APC3 mouse monoclonal (Moravian, 1:500). Mad2 rabbit polyclonal (A300-300A, 1:500; Bethyl Laboratories), Bub3 mouse monoclonal (611731, 1:500; BD Biosciences), BubR1 rabbit polyclonal (A300-995A, 1:1,000; Bethyl Laboratories), BubR1 mouse monoclonal (raised against TPR domain, 1:500, Biotech Research and Innovation Center, Copenhagen).

RNAi and Plasmid transfection.

Endogenous proteins were depleted using RNAi max from Life Technologies according to manufactures instructions. Cdc20 (5'-CGAAAUGACUAUUACCUGA-3', Thermo Fischer siRNA ID s2748), B56 (oligoes as described in Foley et al 2011(Foley et al., 2011)) , BubR1 (5'GAUGGUGAAUUGUGGAAUAdTdT, Sigma). In more detail, for live cell imaging 50 µl transfection mix with 1 µl siRNA Max and 0.25 µl siRNA oligo (stock concentration 10 µmol) in Optimem was added to 200 µl Optimem in 8 Well IBIDI dishes with cells at a confluency of about 80 %. After 2 hours of treatment DMEM containing 20 % FBS was added until medium was changed the next day.

Live cell imaging.

Cells grown on eight-well slides (Ibidi) were cultured in complete DMEM and subjected to a double thymidine block. Cells were transfected with siRNA and plasmid between the two thymidine blocks. Two hours after release from the second thymidine block (or before filming) the medium was changed to L-15 medium (Life Technologies) supplemented with 10 % fetal bovine serum (Hyclone) and nocodazole (30 ng/ml) when indicated. The slide was mounted onto a Delta Vision Elite microscope (GE Healthcare) and cells were filmed for 16 to 24 hours in 4 to 20 minutes intervals using a 40X, 1.35 NA, WD 0.10 objective. All data analysis was performed using the softWoRx software (GE Healthcare).

Purification of Cdc20 and APC4

Cdc20 and APC/C complexes were purified from cells after a double thymidine treatment protocol. HeLa or cells were seeded at 20 % confluency on day 1 treated with siRNA for 5 hours when indicated. After 14 to 18 hours in thymidine cells were released for 8 hours and

when indicated transfected with plasmids. After a second 24-hour thymidine treatment cells were released into nocodazole (200 ng/ml) and harvested by mitotic shake-off. When indicated cells were treated with RO3306 (5 or 10 μM) to force mitotic exit and collected at indicated times. Cells were lysed in lysis buffer (150 mM NaCl, 50 mM Tris-HCl pH 7.8, 1mM DTT, 0.1 % NP40) supplemented with PhosStop and Complete Mini (Roche). Cdc20 or APC/C complexes were immunoprecipitated using a mouse monoclonal Cdc20 (#1 or #2 as in antibody section, #1 was used when not further specified) antibody or mouse monoclonal APC4 antibody cross-linked to Protein G-Sepharose 4B (Life Technologies) for 1 hour at 4° C. Precipitated protein complexes were washed in lysis buffer. Precipitated protein complexes were eluted with 4xLSB (Life Technologies).

Quantitative Infrared Western

All cell lysates and immunoprecipatations were analyzed by Li-Cor quantitative infrared western technology. Proteins were separated by SDS-PAGE and blotted onto Immobilion FL membrane (Millipore). Membranes were incubated with indicated primary antibody and subsequently with IRDye 800 or 680 secondary antibodies (Li-Cor). Membranes were scannend using the Odyssey Sa imaging system (Li-Cor) and quantification was carried out using the Odyssey Sa Application software (Li-Cor).

Expression and purification of proteins

Proteins were produced as described previously in Hein et al 2017 (Hein et al., 2017). In short, full length Arpp19 and derivatives thereof, were cloned into pGEX-4T-1 to generate N-terminally GST-tagged fusion proteins. Constructs were transformed into BL21 (DE3) cells and expression was induced by addition of 0.5 mM IPTG at 37°C for 3 hours. Expression for GST-Arpp19 was induced by addition of 0.5 mM IPTG overnight at 18°C. Bacterial pellets

were resuspended in ice cold lysis buffer (50 mM Tris-HCl pH 7.4, 300 mM NaCl, 10% glycerol, 5 mM β-mercaptoethanol, 1 mM PMSF, and complete EDTA-free Protease Inhibitor Cocktail tablets (Roche)) and lysed in an EmulsiFlex-C3 High Pressure Homogenizer (Avestin). Lysates were cleared at 26,200 g for 30 min at 4°C and supernatants incubated with pre-washed Glutathione Sepharose 4 Fast Flow beads (GE Healthcare) for 90 min at 4°C with mixing. Beads were washed 6 times in ice cold lysis buffer, and GST-fusion proteins eluted at 22°C for 30 min, 1250 rpm in elution buffer (50 mM Tris pH 8.8, 300 mM NaCl, 10% glycerol, 5 mM β-mercaptoethanol, 20 mM reduced glutathione). Eluates were further purified by gelfiltration on a Superdex 75 10/300 GL column. . For expression of MASTL ten 15 cm dishes, seeded with $1x10^7$cells per dish, were transfected with 15 µg FLAG-MASTL plasmid. Cells were collected 2 days after the transfection and FLAG-MASTL was purified by lysing cells in buffer L (350 mM NaCl, 50 mM Tris pH 8.0, 0.05% NP40). Following centrifugation the lysate was incubated with 400 µl anti-FLAG beads (Sigma). The beads were washed with buffer L and FLAG-MASTL was eluted with buffer L containing 200 ng/ul FLAG peptide by incubating for 20 minutes at room temperature. 10 % Glycerol was added and FLAG-MASTL was snap-freezed and stored at -80 °C.

Phosphorylation of GST-Arpp19 with MASTL

Thiophosphorylated GST-Arpp19 was generated as described previously (Hein et al., 2017). In short, purified GST, GST-Arpp19^{wt} or GST-Arpp19^{S62A} was incubated with purified 3xFLAG-MASTL kinase in protein kinase buffer (50 mM Tris-Hcl pH 7.5, 10 mM MgCl2, 0.1 mM EDTA, 2 mM DTT, 0.01% Brij 35) with 500 µM ATP and 1 µCi [γ-32P] ATP at 30°C for 30 min, or with 500 µM ATP□S at 30°C for 60 min for pull-down experiments.

Cell lysate Phosphatase Inhibition Assay

The phosphatase inhibition assay was performed as described previously (Hein et al., 2017). In short, HeLa cells were synchronized in mitosis with nocodazole (200 ng/ml) after double thymidine block. Cells were collected and washed with PBS. Lysis buffer (150 mmol NaCl, 25 mmol Tris, 0.1 % NP40, Complete Protease Inhibitor) containing 1 mmol okadaic acid, 10 ug GST-Arpp19 or Nipp1 was added and immediately transferred to thermomixer for indicated times at 600 rpm and 30 C. Ice cold lysis buffer containing 2x PhosStop inhibitor tablets was added to stop the reaction. Lysis was cleared at 20000g for 15 min at 4 C and Cdc20 or APC4 was immune precipitated and samples analyzed by western-blot using the indicated antibodies. For mass spectrometry analysis the lysates were flash frozen in liquid nitrogen after centrifugation.

Quantitative TMT phosphoproteomics analysis

LxxIxE and AxxAxA peptide treated cell lysates were snap-frozen and proteins were acetone precipitated (Kruse et al., 2020). The precipitated proteins were digested overnight with trypsin (1:100 w/w) at 37°C. Digests were desalted using C_{18} solid-phase extraction cartridges (ThermoFischer Scientific) and dried by vacuum centrifugation. Phospho-peptides were enriched in these samples using High-Select™ Fe-NTA Phosphopeptide Enrichment Kit according to manufacturer's protocol (ThermoFisher Scientific). Phosphopeptides were resuspended in 133 mM HEPES (SIGMA) pH 8.5 and TMT reagent (ThermoFisher Scientific) stored in dry acetonitrile (ACN) (Burdick & Jackson) was added followed by vortexing to mix reagent and peptides. After 1 hr at room temperature, an aliquot was withdrawn to check for labeling efficiency while the remaining reaction was stored at -80°C. Once labeling efficiency was confirmed to be at least 95%, each reaction was quenched with ammonium bicarbonate for 10 minutes, mixed, acidified with 20% TFA, and desalted. The desalted multiplex was dried by vacuum centrifugation and separated by

offline pentafluorophenyl (PFP)-based reversed phase HPLC fractionation as previously described (Grassetti et al., 2017).

TMT-labeled samples were analyzed on an Orbitrap Fusion (Senko et al., 2013) mass spectrometer (ThermoScientific) equipped with an Easy-nLC 1000 (ThermoScientific). Peptides were resuspended in 8% methanol / 1% formic acid across a column (45 cm length, 100 μm inner diameter, ReproSil, C_{18} AQ 1.8 μm 120 Å pore) pulled in-house across a 2 hr gradient from 3% acetonitrile/0.0625% formic acid to 37% acetonitrile/0.0625% formic acid. The Orbitrap Fusion was operated in data-dependent, SPS-MS3 quantification mode (McAlister et al., 2014; Ting et al., 2011) wherein an Orbitrap MS1 scan was taken (scan range = 350 – 1200 m/z, R = 120K, AGC target = 3e5, max ion injection time = 100ms). Followed by data-dependent Orbitrap trap MS2 scans on the most abundant precursors for 3 seconds. Ion selection; charge state = 2: minimum intensity 2e5, precursor selection range 650-1200 m/z; charge state 3: minimum intensity 3e5, precursor selection range 525-1200 m/z; charge state 4 and 5: minimum intensity 5e5). Quadrupole isolation = 0.7 m/z, R = 30K, AGC target = 5e4, max ion injection time = 80ms, CID collision energy = 32%). Orbitrap MS3 scans for quantification (R = 50K, AGC target = 5e4, max ion injection time = 100ms, HCD collision energy = 65%, scan range = 110 – 750 m/z, synchronous precursors selected = 5). The raw data files were searched using COMET with a static mass of 229.162932 on peptide N-termini and lysines and 57.02146 Da on cysteines, and a variable mass of 15.99491 Da on methionines and 79.96633 Da on serines, threonines and tyrosines against the target-decoy version of the human proteome sequence database (UniProt; downloaded 2/2020, 40704 entries of forward and reverse protein sequences) and filtered to a <1% FDR at the peptide level. Quantification of LC-MS/MS spectra was performed using in house developed software (Kruse et al., 2020). Phosphopeptide intensities were adjusted

based on total TMT reporter ion intensity in each channel and $\log_2$ transformed. P-values were calculated using a two-tailed Student's t-test assuming unequal variance.

A

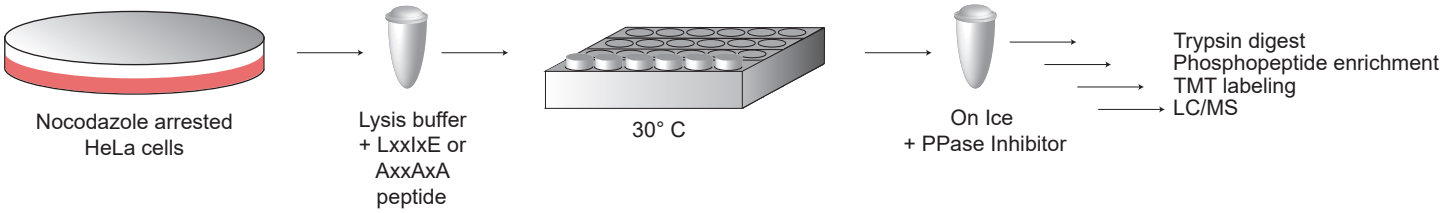

B

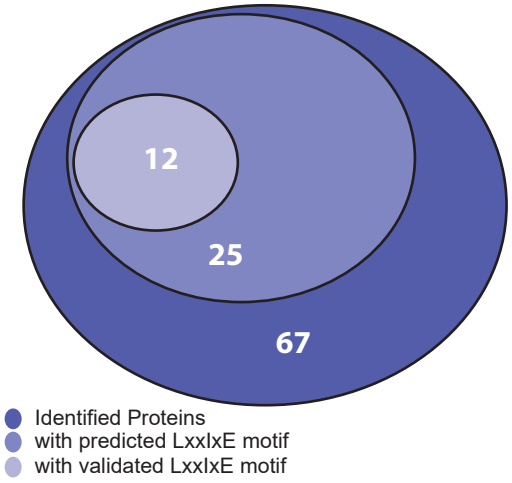

C

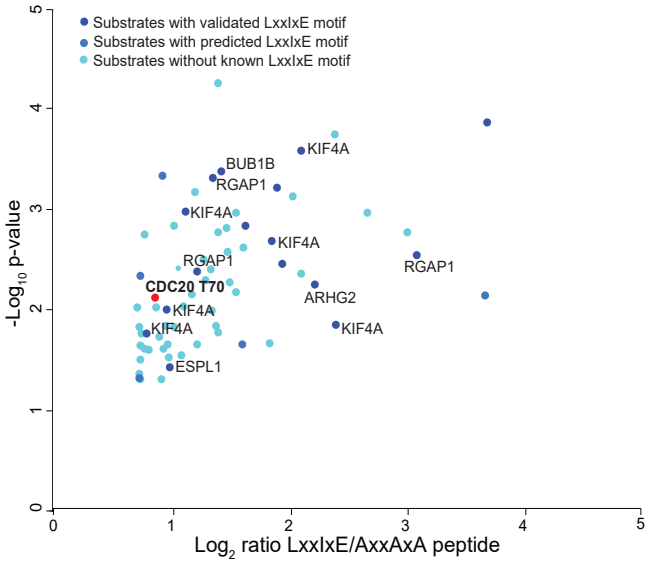

D

Name	Modsites	B56 inh/cont	pvalue	LxxIxE
KIF4A	T799	2.09	0.00	Yes
RGAP1	S203	1.42	0.00	Yes
ESPL1	S1475	0.98	0.03	Yes
ARHG2	S886	2.22	0.00	Yes
BUB1B	T508	1.35	0.00	Yes
ADA17	T735	0.92	0.00	Yes
⋮	⋮	⋮	⋮	⋮
KIF2C	S95	3.67	0.00	Predicted
KIF4B	S1038	3.68	0.00	Predicted
RIF1	S1008	1.46	0.00	Predicted
ZC11A	S290	1.28	0.01	Predicted
⋮	⋮	⋮	⋮	⋮

E

Name	Modsites	B56 inh/cont	pvalue	LxxIxE
LAP2B	T279	2.39	0.00	No
SCRIB	S1508	3.00	0.00	No
REPI1	T287	2.09	0.00	No
REPI1	T482	2.02	0.00	No
CDK17	S180	1.55	0.00	No
REPI1	T510	1.39	0.03	No
CDK18	S89	1.48	0.00	No
PHF14	S290	1.37	0.01	No
NAB1	S103	1.34	0.02	No
SYMPK	S494	1.27	0.01	No
⋮	⋮	⋮	⋮	⋮
CDC20	T70	0.85	0.02	No
⋮	⋮	⋮	⋮	⋮

Figure 1

A

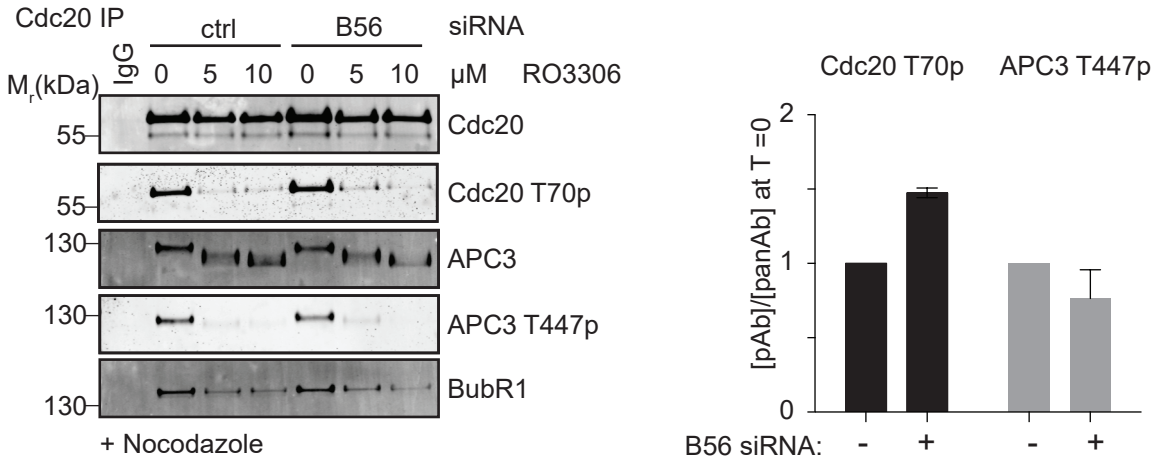

B

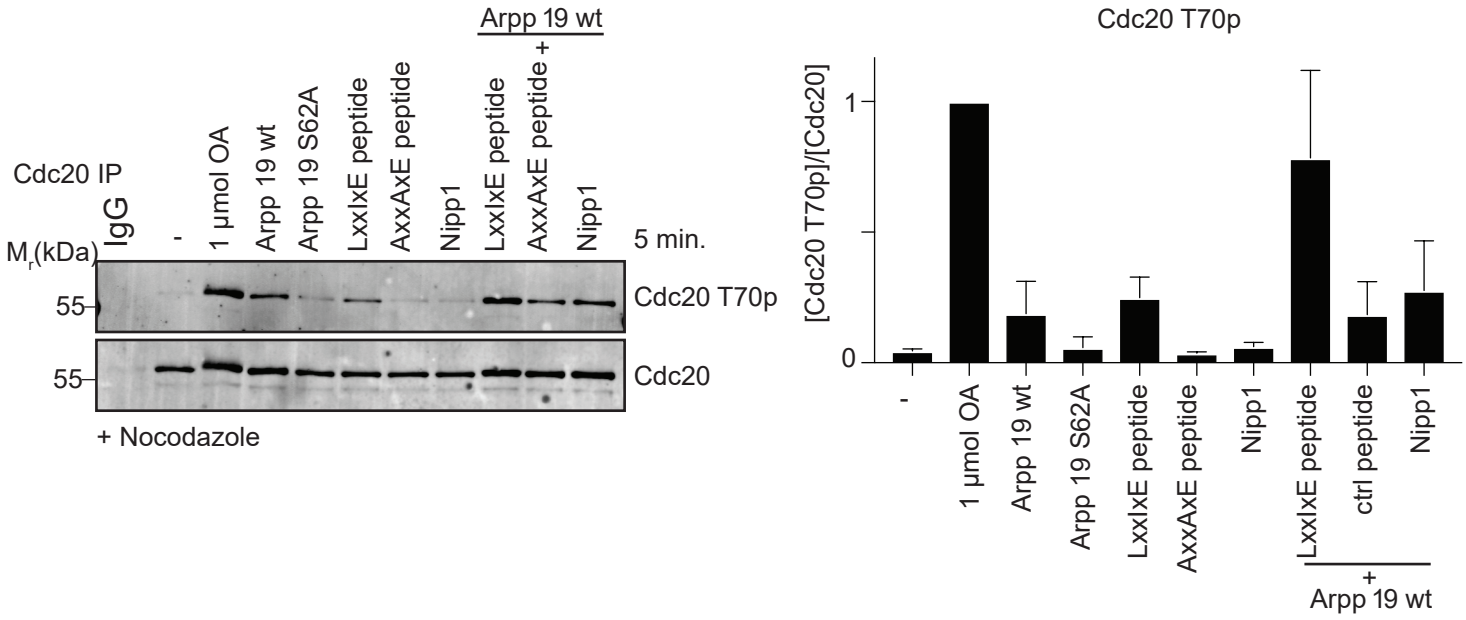

C

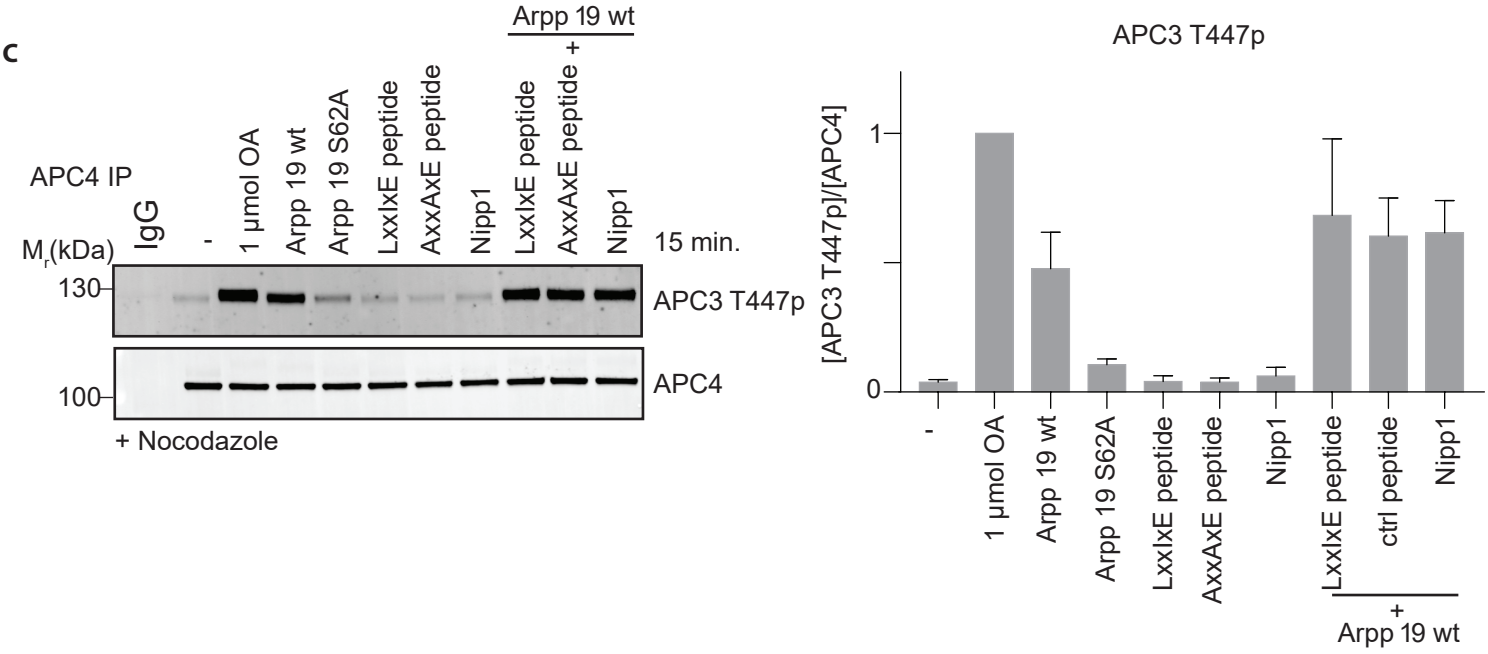

Figure 2

A

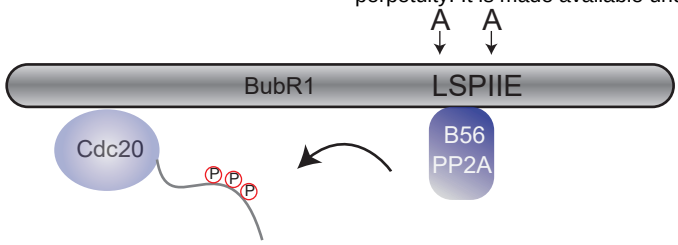

B

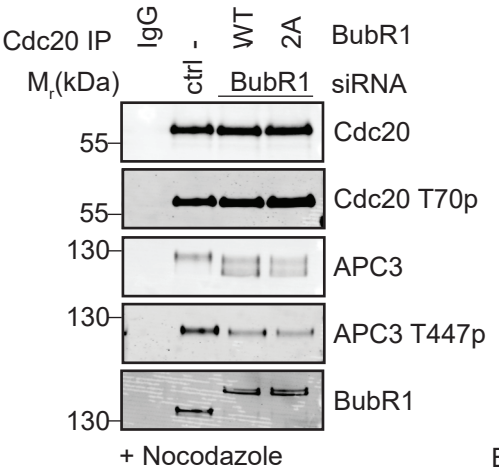

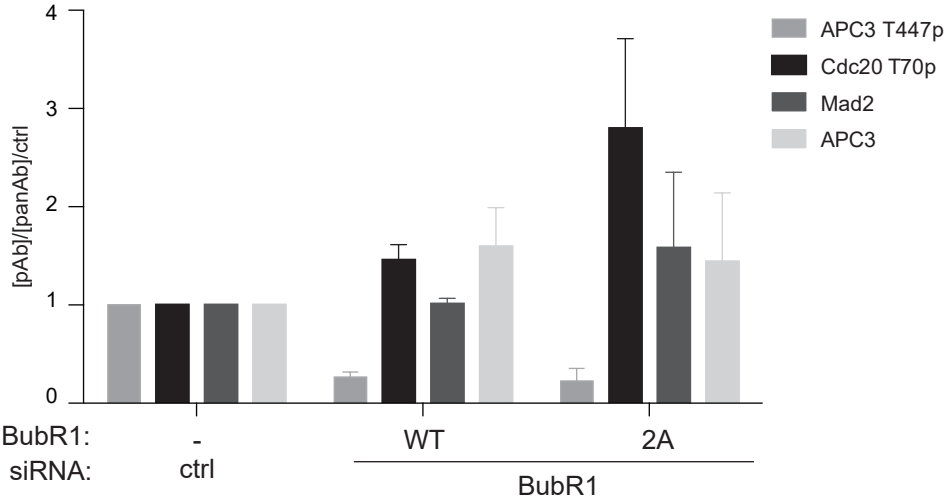

C

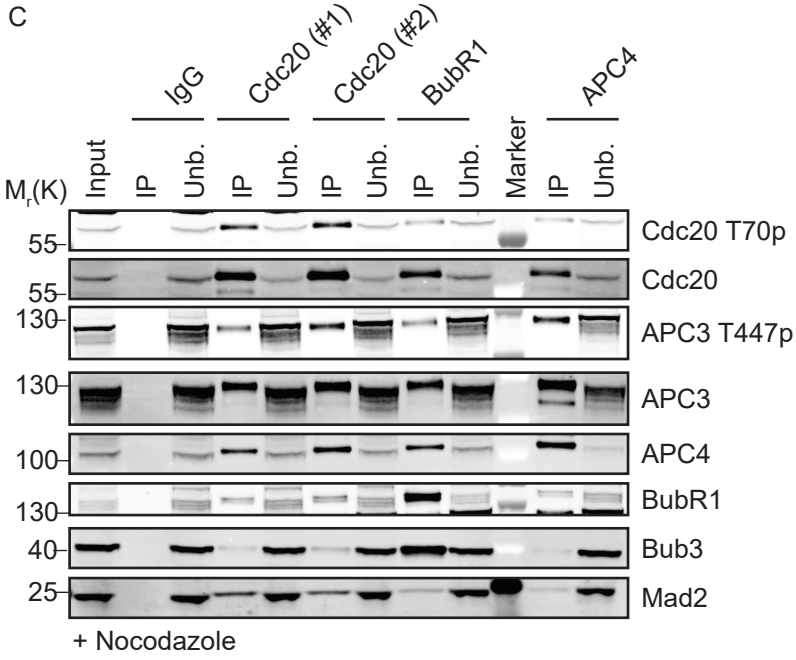

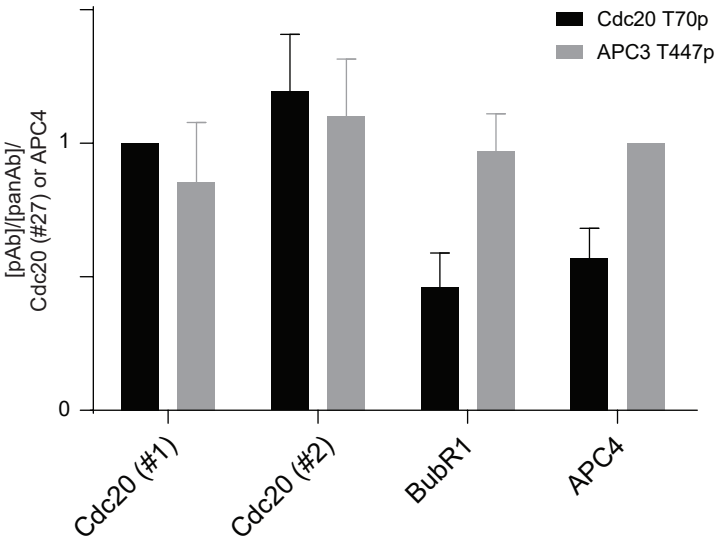

Figure 3

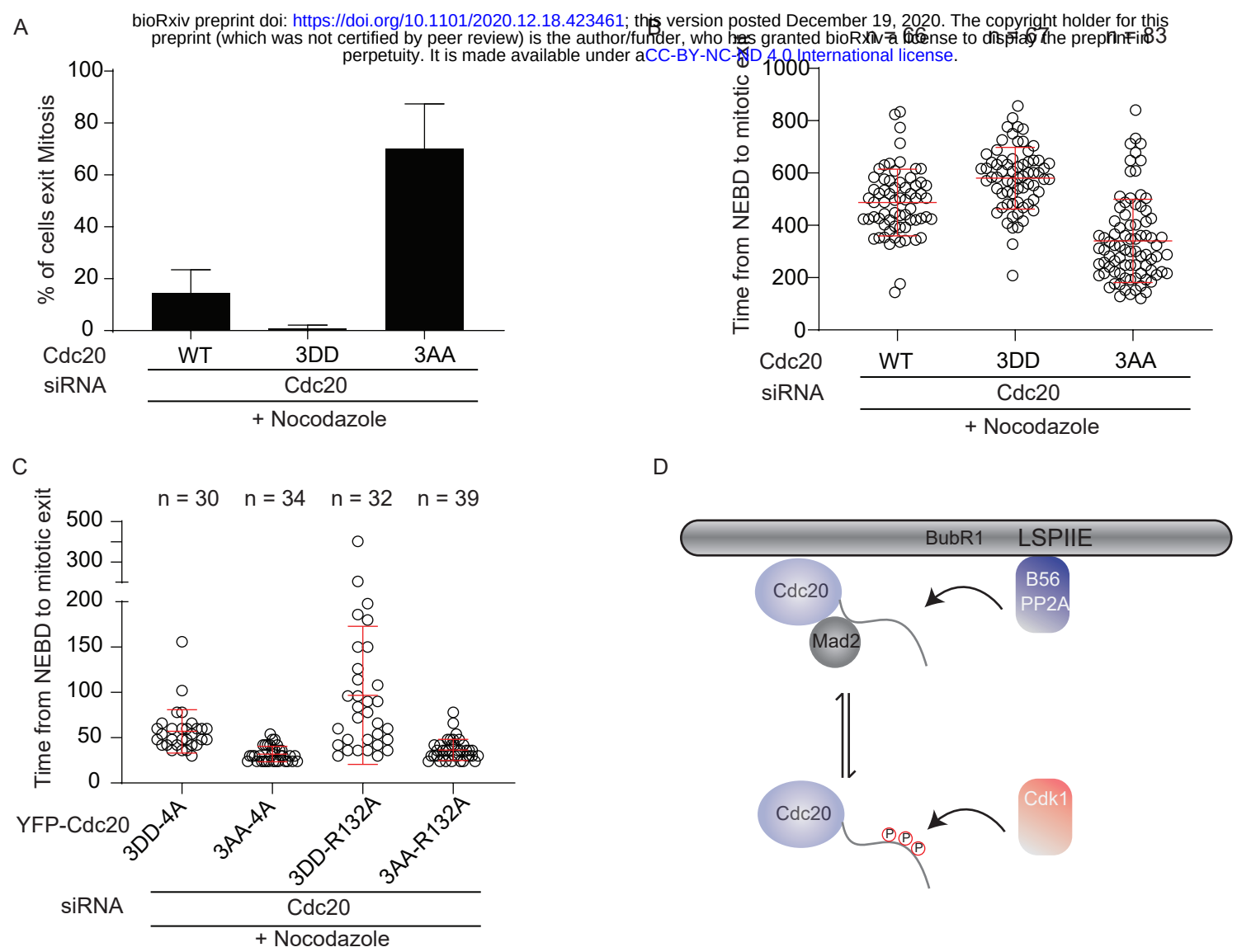

Figure 4

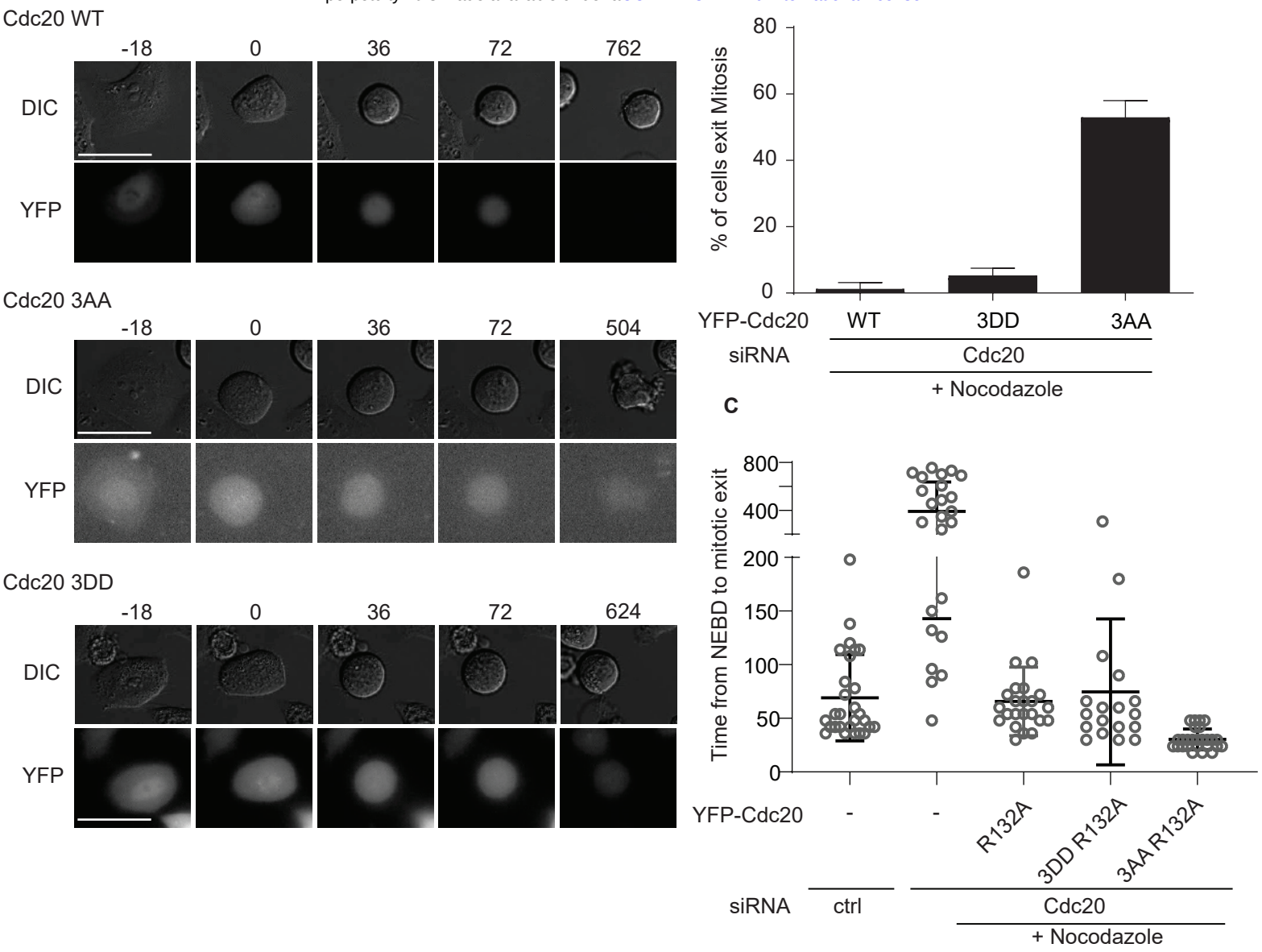

Supplementary Figure 1